Supporting Information for

Crystallographic Characterization of Y_2C_{2n} (2n = 82, 88-94): Direct Y-Y Bonding and Cage-Dependent Cluster Evolution

Changwang Pan,‡[a] Wangqiang Shen,‡[a] Le Yang,‡[b] Lipiao Bao,[a] Zhan Wei,[b] Peng Jin,*[b] Hongyun Fang,*[a] Yunpeng Xie,*[a] Takeshi Akasaka[a] and Xing Lu*[a]

[a] *State Key Laboratory of Materials Processing and Die & Mould Technology, School of Materials Science and Engineering, Huazhong University of Science and Technology, 1037 Luoyu Road, Wuhan, 430074 China. E-mail:* lux@hust.edu.cn.

[b] *School of Materials Science and Engineering, Hebei University of Technology, Tianjin, 300130 China. E-mail:* china.peng.jin@gmail.com

‡ These authors contributed equally to this work.

Table of Contents

General instruments. High performance liquid chromatography (HPLC) was conducted on an LC-908 machine (Japan Analytical Industry Co., Ltd.). Laser desorption ionization time-of-flight (LDI-TOF) mass spectrometry was measured on a Microflex spectrometer (Bruker Daltonics Inc., Germany). Vis-NIR spectra were obtained with a PE Lambda 750S spectrophotometer (PerkinElmer, America) in carbon disulfide.

Computational details. With increased fullerene size, the number of cage isomers grows dramatically. To quickly find the parent cage of an EMF molecule, a well-accepted and efficient strategy is to screen the low-energy empty cages with appropriate negative charges. Since the internal Y_2 and Y_2C_2 may formally donate four or six electrons to the fullerene cage, the reported low-lying tetra-anions and hexa-anions of the corresponding fullerene isomers were selected to form $Y_2@C_{2n}$ or $Y_2C_2@C_{2n-2}$.[S1-S6] Therefore, 7, 8, 6, 8 and 8 isomers were considered for Y_2C_{82}, Y_2C_{88}, Y_2C_{90}, Y_2C_{92}, and Y_2C_{94}, respectively. For each isomer, various positions and orientations for the internal species were fully considered during the structural optimization, and only the lowest-energy conformation was reported.

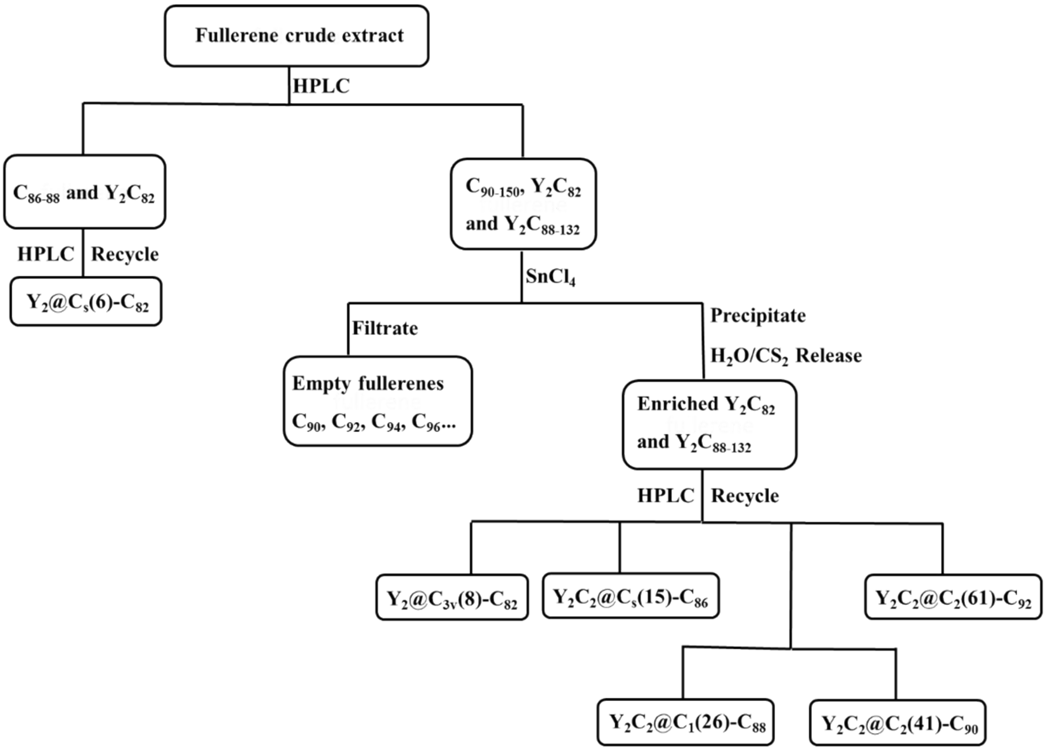

Figure S1. Isolation scheme of $Y_2@C_s(6)\text{-}C_{82}$, $Y_2@C_{3v}(8)\text{-}C_{82}$, $Y_2C_2@C_s(15)\text{-}C_{86}$, $Y_2C_2@C_1(26)\text{-}C_{88}$, $Y_2C_2@C_2(41)\text{-}C_{90}$, and $Y_2C_2@C_2(61)\text{-}C_{92}$.

Y_2C_{2n} ($2n$ = 82, 88-94) isomers were synthesized by a direct-current arc discharge method and were obtained through a combinational process involving Lewis-acid treatment and high performance liquid chromatography (HPLC) separations. Figure S1 overviews the experimental procedures for the separation and purification of Y_2C_{2n} ($2n$ = 82, 88-94) isomers.

The crude extraction was injected into a 5PYE column with toluene as eluent and *o*-dichlorobenzene (*o*-DCB) was injected to wash out the higher fullerenes after 55 min, and five fractions (F-1, F-2, F-3, F-4 and F-o) were obtained (Figure S2a). Fraction F-1 was then separated on a Buckyprep column and fraction F-1-1 corresponding to $Y_2@C_s(6)$-C_{82} obtained (Figure S2b). The other four fractions (F-2, F-3, F-4 and F-o) were treated with $SnCl_4$ which leaded to the rapid enrichment of $SnCl_4$-EMF complexes as precipitates, which easily decompose to provide pure Y_2C_{2n}-type EMF powders by a simple water treatment. Subsequently, the powders were dissolved in a CS_2 solution. These solutions were dried by a rotary evaporator, and the respective solid residue was dissolved in toluene and filtered to get the clear solution containing the corresponding EMFs (named as, F-2p, F-3p, F-4p and F-op, respectively). The mass spectra of F-2p, F-3p, F-4p and F-op show that empty fullerenes have been completely removed by the treatment with $SnCl_4$ (Figure S3). Further details for the separation of $Y_2@C_{3v}(8)$-C_{82}, $Y_2C_2@C_s(15)$-C_{86}, $Y_2C_2@C_1(26)$-C_{88}, $Y_2C_2@C_2(41)$-C_{90}, and $Y_2C_2@C_2(61)$-C_{92} are given below.

Then, F-2p was injected into a 5PYE column with toluene as eluent and fraction F-2p-1 corresponding to pure $Y_2@C_{3v}(8)$-C_{82} was collected (Figure S4a). F-3p was separated through a two-step HPLC separation with chlorobenzene as eluent. The first step was performed on a Buckyprep-M column and fraction F-3p-1 was then injected into a 5PBB column with chlorobenzene as eluent, and fraction F-3p-1-1 ($Y_2C_2@C_s(15)$-C_{86}) was finally collected (Figures S4b and S4c). The separation of F-4p was conducted through recycling HPLC with a 5PBB column, and three fractions F-4p-1 ($Y_2C_2@C_2(43)$-C_{90}) and F-4p-2 ($Y_2C_2@C_1(26)$-C_{88}) were obtained (Figure S4d).

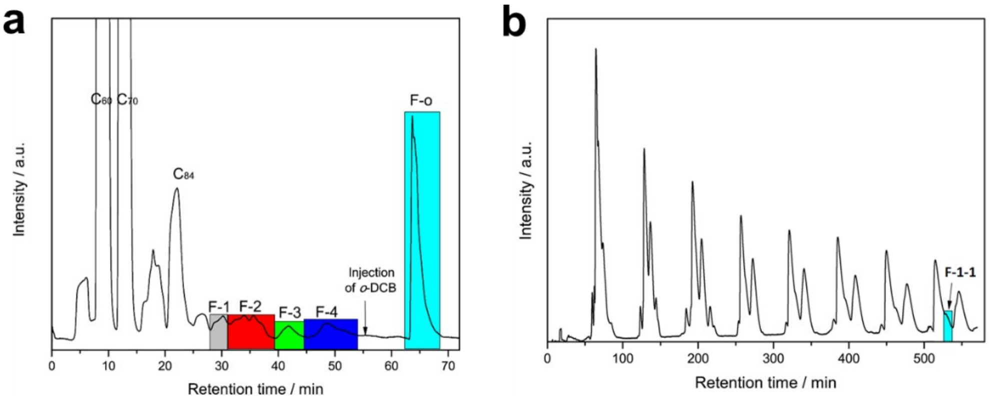

Figure S2. Isolation of F-1-1 ($Y_2@C_s(6)$-C_{82}). HPLC chromatograms of (a) the crude extraction obtained by a 5PYE column, (b) F-1-1 obtained by a Buckyprep column. Conditions: Φ = 20 mm × 250 mm, eluent = toluene, flow rate = 9.99 mL/min, detection wavelength = 330 nm, room temperature.

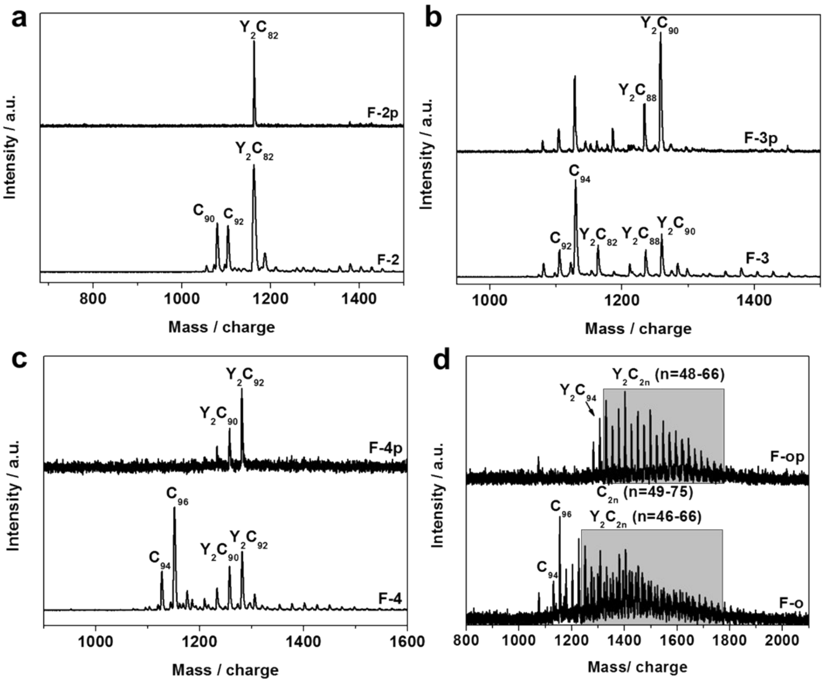

Figure S3. Mass spectra of (a) F-2 and F-2p, (b) F-3 and F-3p, (c) F-4 and F-4p and (d) F-o and F-op.

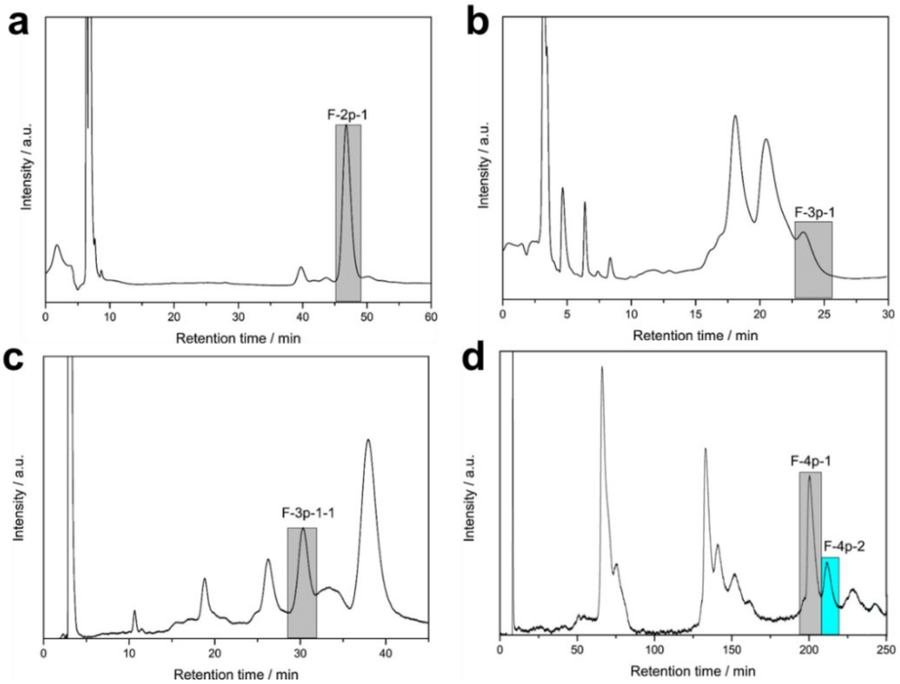

Figure S4. Isolation of F-2p-1 ($Y_2@C_{3v}(8)$-C_{82}), F-3p-1-1 ($Y_2C_2@C_s(15)$-C_{86}), F-4p-1 ($Y_2C_2@C_1(26)$-C_{88}), and F-4p-2 ($Y_2C_2@C_2(41)$-C_{90}). HPLC chromatograms of (a) F-2p-1 obtained by a 5PYE column with λ = 330 nm, a flow rate of 10 mL/min, and toluene as the eluent at room temperature. (b) F-3p-1 obtained by a Buckyprep-M column, (c) F-3p-1-1 obtained by a 5PBB column, (d) F-4p-1 and F-4p-2 obtained by a 5PBB column. Conditions: Φ = 20 mm × 250 mm, eluent = chlorobenzene, flow rate = 9.99 mL/min, detection wavelength = 330 nm, room temperature.

Fraction F-op was separated through a four-step HPLC separation with chlorobenzene as eluent. In detail, the first-step separation was performed on a Buckyprep column (Figure S5a) and then fraction F-op-1 was separated with a 5PBB column to get fraction F-op-1-1 (Figure S5b). At the third step, fraction F-op-1-1 was injected into a Buckyprep-M Column and F-op-1-1-1 was collected (Figure S5c). Finally, fraction F-op-1-1-1 was injected into a 5PYE column, and fraction F-op-1-1-1-1 ($Y_2C_2@C_2(61)$-C_{92}) was obtained (Figure S5d). The analytical HPLC chromatograms and the laser-desorption/ionization time-of-flight (LDI-TOF) mass spectra of these endohedrals are shown in Figures S6 and S7.

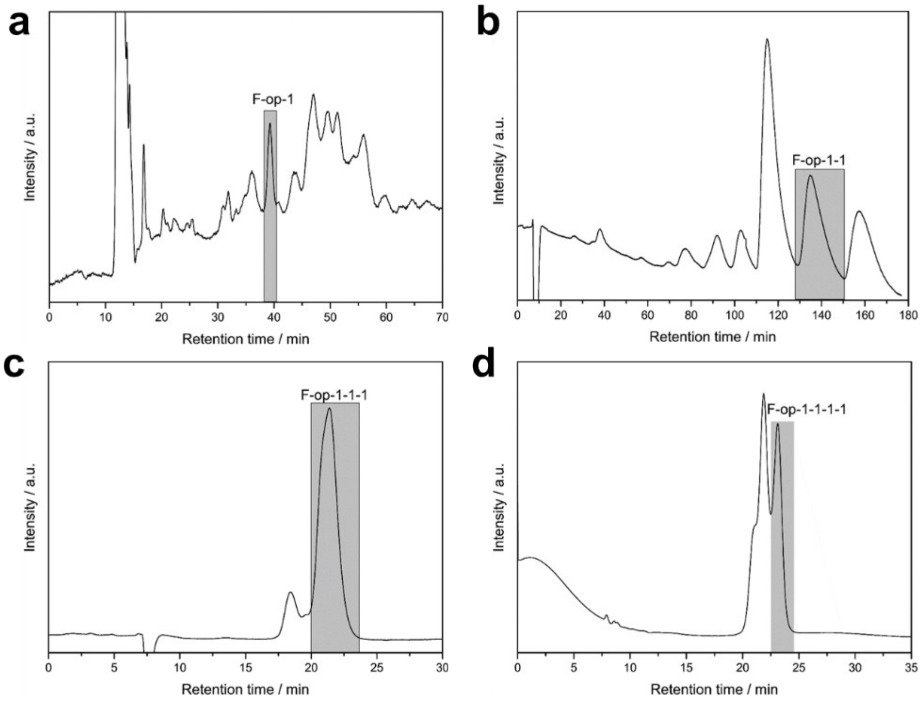

Figure S5. Isolation schemes of F-op-1-1-1-1 ($Y_2C_2@C_2(61)$-C_{92}). HPLC chromatograms of (a) F-op-1 obtained by a Buckyprep column, (b) F-op-1-1 obtained by a 5PBB column, (c) F-op-1-1-1 obtained by a Buckyprep-M column, (d) F-op-1-1-1-1 obtained by a 5PYE column. Conditions: Φ = 20 mm × 250 mm, eluent = chlorobenzene, flow rate = 9.99 mL/min, detection wavelength = 330 nm, room temperature.

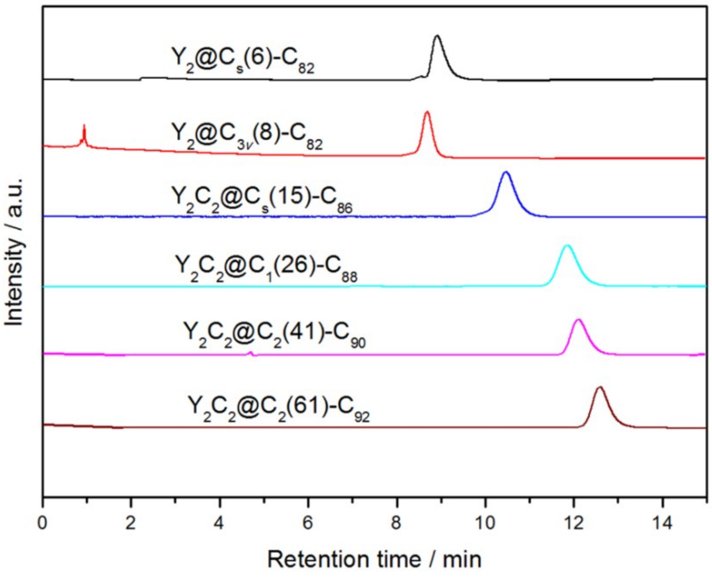

Figure S6. Analytical HPLC profiles with chlorobenzene as eluent of $Y_2@C_s(6)$-C_{82}, $Y_2@C_{3v}(8)$-C_{82}, $Y_2C_2@C_s(15)$-C_{86}, $Y_2C_2@C_1(26)$-C_{88}, $Y_2C_2@C_2(41)$-C_{90}, and $Y_2C_2@C_2(61)$-C_{92}. HPLC conditions: Buckyprep column; 1.0 mL/min flow, 330 nm detection wavelength, 40 °C.

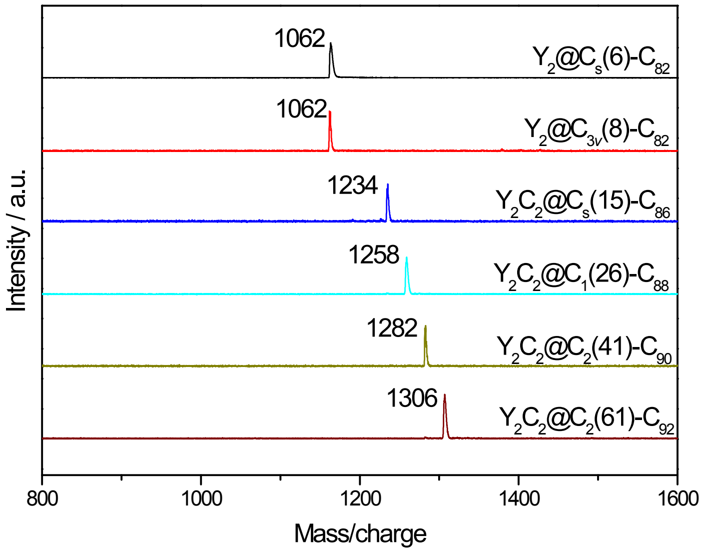

Figure S7. Mass spectra of $Y_2@C_s(6)$-C_{82}, $Y_2@C_{3v}(8)$-C_{82}, $Y_2C_2@C_s(15)$-C_{86}, $Y_2C_2@C_1(26)$-C_{88}, $Y_2C_2@C_2(41)$-C_{90}, and $Y_2C_2@C_2(61)$-C_{92}.

Table S1. Crystallographic data of Y_2C_{2n} (2n = 82, 88-94) isomers.

Compound	**$Y_2@$ $C_s(6)$-C_{82}**	**$Y_2@$ $C_{3v}(8)$-C_{82}**	**$Y_2C_2@$ $C_s(15)$-C_{86}**	**$Y_2C_2@$ $C_1(26)$-C_{88}**	**$Y_2C_2@$ $C_2(41)$-C_{90}**	**$Y_2C_2@$ $C_2(61)$-C_{82}**
crystal system	monoclinic	monoclinic	monoclinic	monoclinic	monoclinic	monoclinic
space group	C2/m	C2/m	C2/m	C2/m	C2/m	C2/m
λ/Å	0.82653	0.71073	0.65250	0.71073	0.65250	0.65250
a/ Å	25.3744(9)	25.2629(12)	23.4570(19)	25.436(5)	23.544(3)	24.3282(7)
b/ Å	15.1207(6)	15.5570(7)	14.3210(12)	15.433(3)	14.4883(18)	17.8364(6)
c/ Å	19.8806(8)	19.4478(9)	18.5441(18)	20.238(4)	18.621(3)	19.1972(6)
α / deg	90	90	90	90	90	90
β / deg	94.306 (10)	94.5570(10)	93.976(2)	92.993(6)	93.714(3)	91.9020(10)
γ / deg	90	90	90	90	90	90
V/ Å^3	7606.2(5)	7619.1(6)	6214.5(9)	7934(3)	6338.3(14)	8325.6(5)
Z	4	4	4	4	4	4
R1 (obsd)	0.1156	0.0676	0.0996	0.1066	0.0966	0.1308
wR2 (obsd)	0.2949	0.1794	0.2864	0.2841	0.2540	0.3404

Table S2. Occupancy values of the internal species inside Y_2C_{2n} (2n = 82, 88-94) cages.

EMFs	C_2 unit	Fractional occupancy of Y site								
Y_2@C_s(6)-C_{82}	Non	Y1/Y1A	Y2/Y2A	Y3/Y3A	Y4/Y4A	Y5/Y5A	Y6/Y6A	Y7	Y8	
		0.24	0.18	0.15	0.14	0.11	0.07	0.11	0.11	
Y_2@C_{3v}(8)-C_{82}	Non	Y1/Y1A	Y2/Y2A	Y3/Y3A	Y4/Y4A					
		0.27	0.23	0.33	0.17					
Y_2C_2@C_s(15)-C_{86}	1	Y1/Y1A	Y2/Y2A							
		0.5	0.5							
Y_2C_2@C_1(26)-C_{88}	1	Y1/Y1A	Y2/Y2A							
		0.5	0.5							
Y_2C_2@C_2(41)-C_{90}	1	Y1/Y1A	Y2/Y2A	Y3/Y3A	Y4/Y4A					
		0.46	0.23	0.17	0.14					
Y_2C_2@C_2(61)-C_{92}	1	Y1/Y1A	Y2/Y2A	Y3	Y4/Y4A	Y5/Y5A	Y6/Y6A	Y7/Y7A	Y8/Y8A	Y9/Y9A
		0.12	0.12	0.08	0.19	0.12	0.15	0.08	0.07	0.11

The atom with a suffix ‘A’ is generated by crystallographic operation.

Table S3. Ni-cage distance, major Y-Y distance, the shortest Y-cage distance, internal Y-C distance range, internal C-C distance and major Y-C_2-Y angel in Y_2@C_s(6)-C_{82}, Y_2@C_{3v}(8)-C_{82}, Y_2C_2@C_s(15)-C_{86}, Y_2C_2@C_1(26)-C_{88}, Y_2C_2@C_2(41)-C_{90}, and Y_2C_2@C_2(61)-C_{92}.

EMFs	Ni-cage distance (Å)	Y-Y distance (Å)	Y-Cage Distance (Å)	Y-C distance (Å)	C-C distance (Å)	Y-C_2-Y angle
Y_2@C_s(6)-C_{82}	2.911	3.635	2.321	-	-	-
Y_2@C_{3v}(8)-C_{82}	2.894	3.596	2.357	-	-	-
Y_2C_2@C_s(15)-C_{86}	2.824	4.121	2.203	2.078-2.316	1.078	145.97°
Y_2C_2@C_1(26)-C_{88}	3.027	4.271	2.041	2.114-2.509	1.131	136.23°
Y_2C_2@C_2(41)-C_{90}	2.736	4.024	2.010	2.034-2.559	1.052	145.32°
Y_2C_2@C_2(61)-C_{92}	2.947	4.349	2.042	2.279-2.608	1.046	137.32°

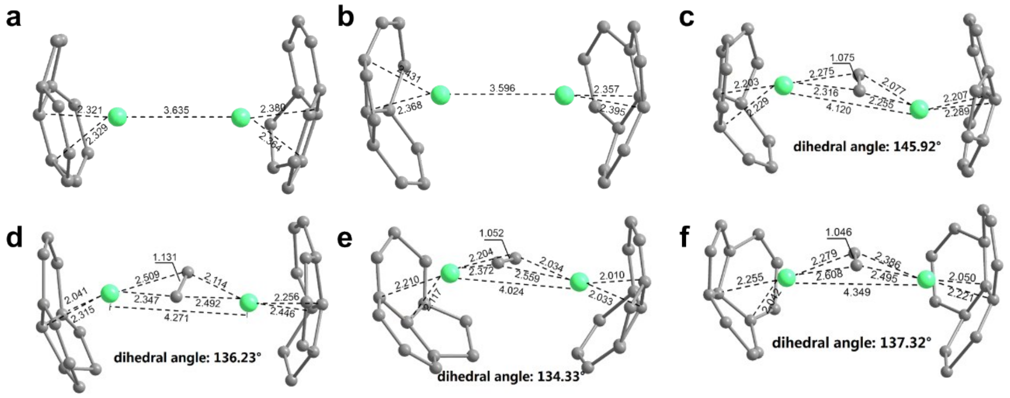

Figure S8. Location of the major Y_2/Y_2C_2 site relative to a cage orientation in (a) $Y_2@C_s(6)\text{-}C_{82}$, (b) $Y_2@C_{3v}(8)\text{-}C_{82}$, (c) $Y_2C_2@C_s(15)\text{-}C_{86}$, (d) $Y_2C_2@C_1(26)\text{-}C_{88}$, (e) $Y_2C_2@C_2(41)\text{-}C_{90}$, and (f)$Y_2C_2@C_2(61)\text{-}C_{92}$.

Table S4. The details of the Vis-NIR absorptions of Y_2C_{2n} (2n = 82, 88-94) isomers.

Metallofullerene	Distinct absorption (nm)	Onset (nm)	Optical bandgap (eV)[a]
$Y_2@C_s(6)\text{-}C_{82}$	475, 622, 709, 786	1385	0.90
$Y_2@C_{3v}(8)\text{-}C_{82}$	720, 908	1097	1.13
$Y_2C_2@C_s(15)\text{-}C_{86}$	780, 1210	1730	0.72
$Y_2C_2@C_1(26)\text{-}C_{88}$	616, 891, 1240	1370	0.91
$Y_2C_2@C_2(41)\text{-}C_{90}$	1035, 1363	1450	0.86
$Y_2C_2@C_2(61)\text{-}C_{92}$	511, 591, 914	1270	0.98

[a]Optical bandgap (eV) ≈ 1240/onset (nm)

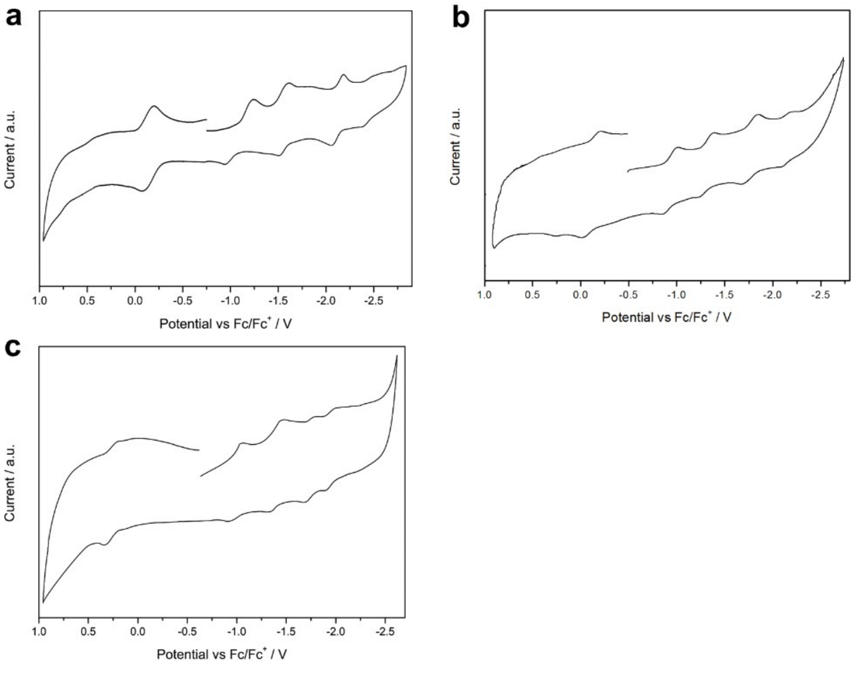

Figure S9. Cyclic voltammograms of (a)$Y_2@C_{3v}(8)\text{-}C_{82}$, (b) $Y_2@C_s(6)\text{-}C_{82}$, and (c) $Y_2C_2@C_2(61)\text{-}C_{92}$ in 0.05 M *n*-Bu_4NPF_6/*o*-DCB solution.

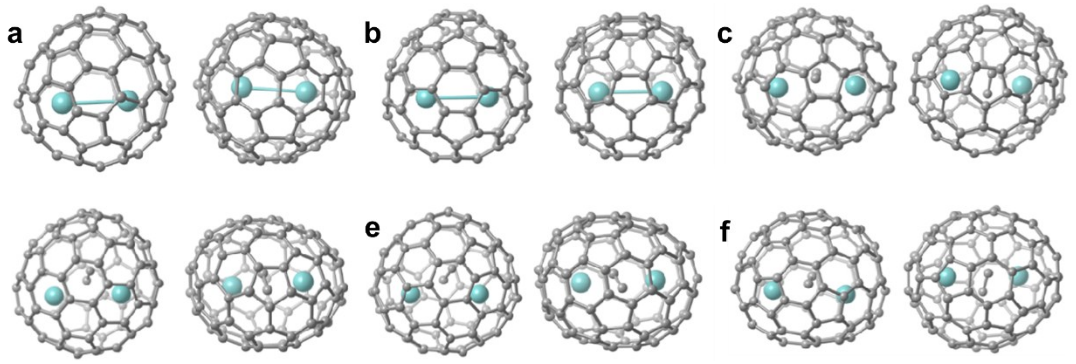

Figure S10. Optimized structures of (a) Y_2@C_s(6)-C_{82}, (b) Y_2@C_{3v}(8)-C_{82}, (c) Y_2C_2@C_s(15)-C_{86}, (d) Y_2C_2@C_1(26)-C_{88}, (e) Y_2C_2@C_2(41)-C_{90}, and (f)Y_2C_2@C_2(61)-C_{92}.

Table S5. Interatomic distances ($R_{\text{Y-Y}}$, Å), Wiberg bond orders (WBOs), electron occupancies (Occ., *e*), natural population analysis charges and natural electron configuration populations of the two Y atoms of experimentally obtained Y_2C_{2n} isomers. The Y atoms are numbered from left to right in Figure 4.

Species	$R_{\text{Y-Y}}$	WBO	Occ.	Atom	Charge	Population	Hybrid composition
Y_2@C_s(6)-C_{82}	3.60	1.11	1.97	Y1	1.08	$5s^{0.49}4d^{0.58}5p^{0.66}6s^{0.01}6p^{0.01}6d^{0.22}$	s(42%)p(39%)d(19%)
				Y2	1.14	$5s^{0.50}4d^{0.56}5p^{0.63}6s^{0.01}6p^{0.01}6d^{0.21}$	s(44%)p(37%)d(19%)
Y_2@C_{3v}(8)-C_{82}	3.54	1.12	1.97	Y1	1.13	$5s^{0.49}4d^{0.56}5p^{0.63}6s^{0.01}6p^{0.01}6d^{0.21}$	s(43%)p(38%)d(19%)
				Y2	1.13	$5s^{0.49}4d^{0.57}5p^{0.62}6s^{0.01}6p^{0.01}6d^{0.21}$	s(43%)p(38%)d(19%)
Y_2C_2@C_s(15)-C_{86}	4.53	0.32		Y1	1.44	$5s^{0.17}4d^{0.69}5p^{0.35}6s^{0.02}6p^{0.12}6d^{0.17}$	
				Y2	1.29	$5s^{0.17}4d^{0.41}5p^{0.24}6s^{0.01}6p^{0.29}6d^{0.20}$	
Y_2C_2@C_1(26)-C_{88}	4.25	0.33		Y1	1.50	$5s^{0.15}4d^{0.69}5p^{0.44}6s^{0.01}6p^{0.01}6d^{0.19}$	
				Y2	1.38	$5s^{0.17}4d^{0.74}5p^{0.36}6s^{0.01}6p^{0.14}6d^{0.23}$	
Y_2C_2@C_2(41)-C_{90}	4.40	0.29		Y1	1.58	$5s^{0.13}4d^{0.67}5p^{0.30}6s^{0.01}6p^{0.12}6d^{0.17}$	
				Y2	1.44	$5s^{0.15}4d^{0.73}5p^{0.34}6s^{0.01}6p^{0.12}6d^{0.17}$	
Y_2C_2@C_2(61)-C_{92}	4.56	0.30		Y1	1.44	$5s^{0.16}4d^{0.69}5p^{0.47}6s^{0.02}6p^{0.01}6d^{0.17}$	
				Y2	1.46	$5s^{0.16}4d^{0.68}5p^{0.46}6s^{0.01}6p^{0.01}6d^{0.17}$	

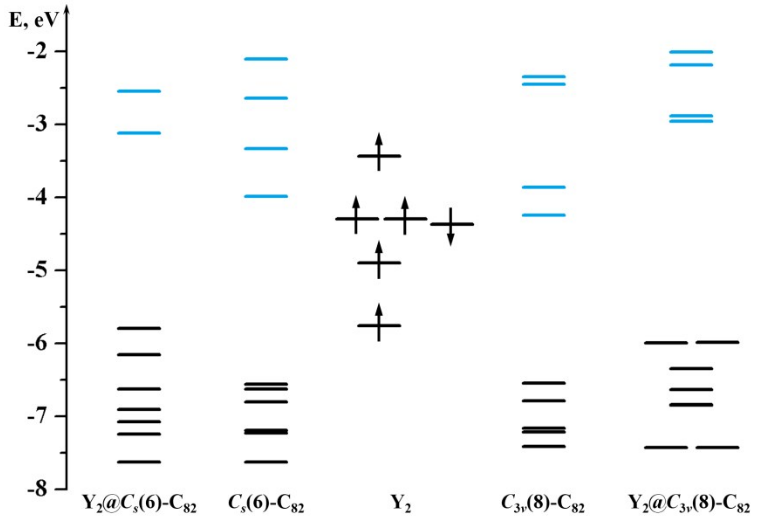

Figure S11. Molecular orbitals of Y_2, C_{82} and $Y_2@C_{82}$ (M06-2X/6-31G*~SDD level). Occupied and unoccupied orbitals are in black and blue, respectively.

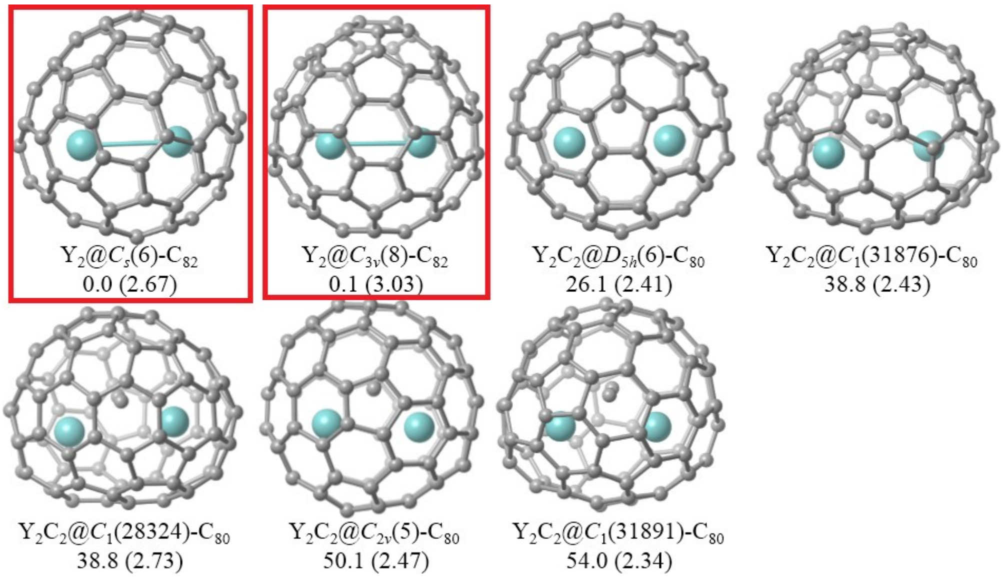
$Y_2@C_s(6)$-C_{82}
0.0 (2.67)
$Y_2@C_{3v}(8)$-C_{82}
0.1 (3.03)
$Y_2C_2@D_{5h}(6)$-C_{80}
26.1 (2.41)
$Y_2C_2@C_1(31876)$-C_{80}
38.8 (2.43)
$Y_2C_2@C_1(28324)$-C_{80}
38.8 (2.73)
$Y_2C_2@C_{2v}(5)$-C_{80}
50.1 (2.47)
$Y_2C_2@C_1(31891)$-C_{80}
54.0 (2.34)

Figure S12. Optimized structures of low-energy Y_2C_{82} isomers with relative energies (kcal/mol) and HOMO-LUMO gap energies (eV, in parenthesis). The isomers marked with red boxes are experimentally obtained.

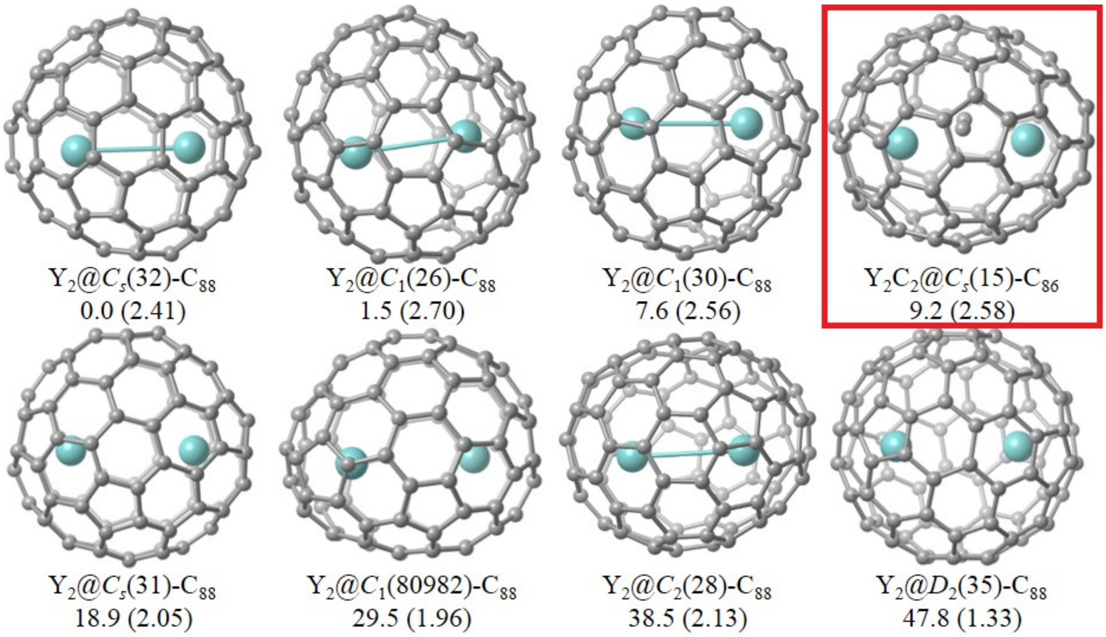

$Y_2@C_s(32)$-C_{88} 0.0 (2.41)

$Y_2@C_1(26)$-C_{88} 1.5 (2.70)

$Y_2@C_1(30)$-C_{88} 7.6 (2.56)

$Y_2C_2@C_s(15)$-C_{86} 9.2 (2.58)

$Y_2@C_s(31)$-C_{88} 18.9 (2.05)

$Y_2@C_1(80982)$-C_{88} 29.5 (1.96)

$Y_2@C_2(28)$-C_{88} 38.5 (2.13)

$Y_2@D_2(35)$-C_{88} 47.8 (1.33)

Figure S13. Optimized structures of low-energy Y_2C_{88} isomers with relative energies (kcal/mol) and HOMO-LUMO gap energies (eV, in parenthesis). The isomer marked with a red box is experimentally obtained.

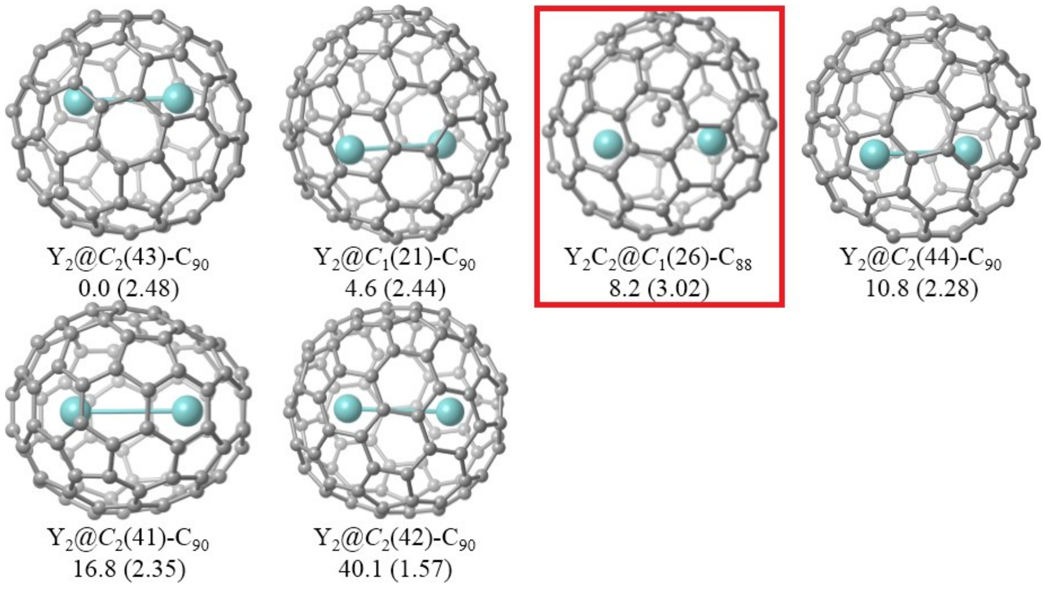

$Y_2@C_2(43)$-C_{90} 0.0 (2.48)

$Y_2@C_1(21)$-C_{90} 4.6 (2.44)

$Y_2C_2@C_1(26)$-C_{88} 8.2 (3.02)

$Y_2@C_2(44)$-C_{90} 10.8 (2.28)

$Y_2@C_2(41)$-C_{90} 16.8 (2.35)

$Y_2@C_2(42)$-C_{90} 40.1 (1.57)

Figure S14. Optimized structures of low-energy Y_2C_{90} isomers with relative energies (kcal/mol) and HOMO-LUMO gap energies (eV, in parenthesis). The isomer marked with a red box is experimentally obtained.

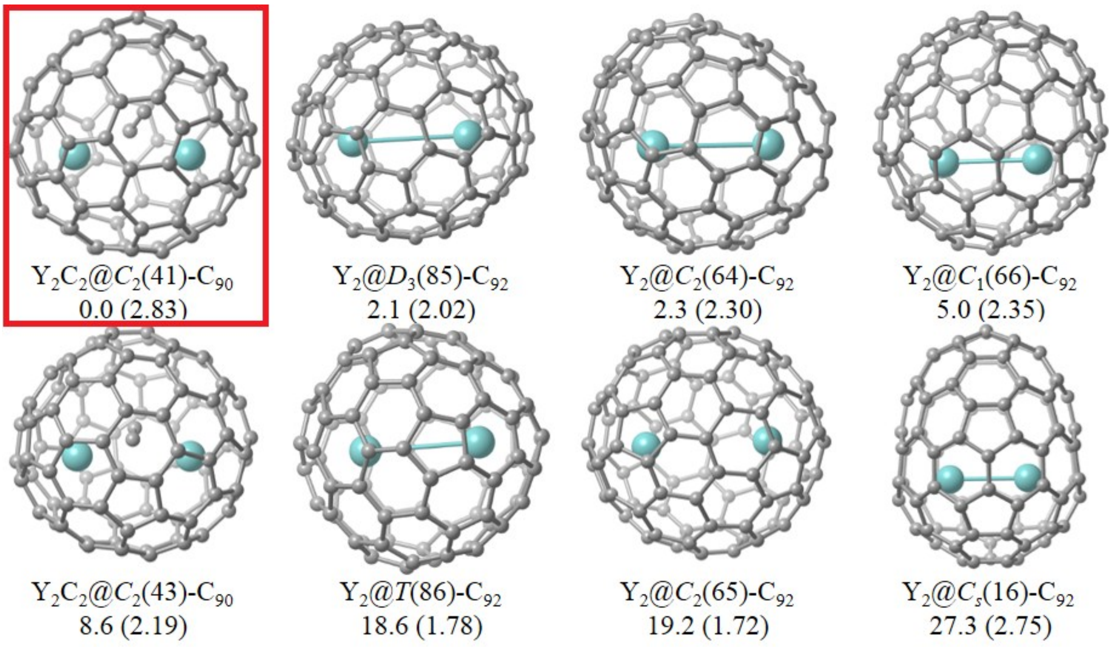

Figure S15. Optimized structures of low-energy Y_2C_{92} isomers with relative energies (kcal/mol) and HOMO-LUMO gap energies (eV, in parenthesis). The isomers marked with red boxes are experimentally obtained.

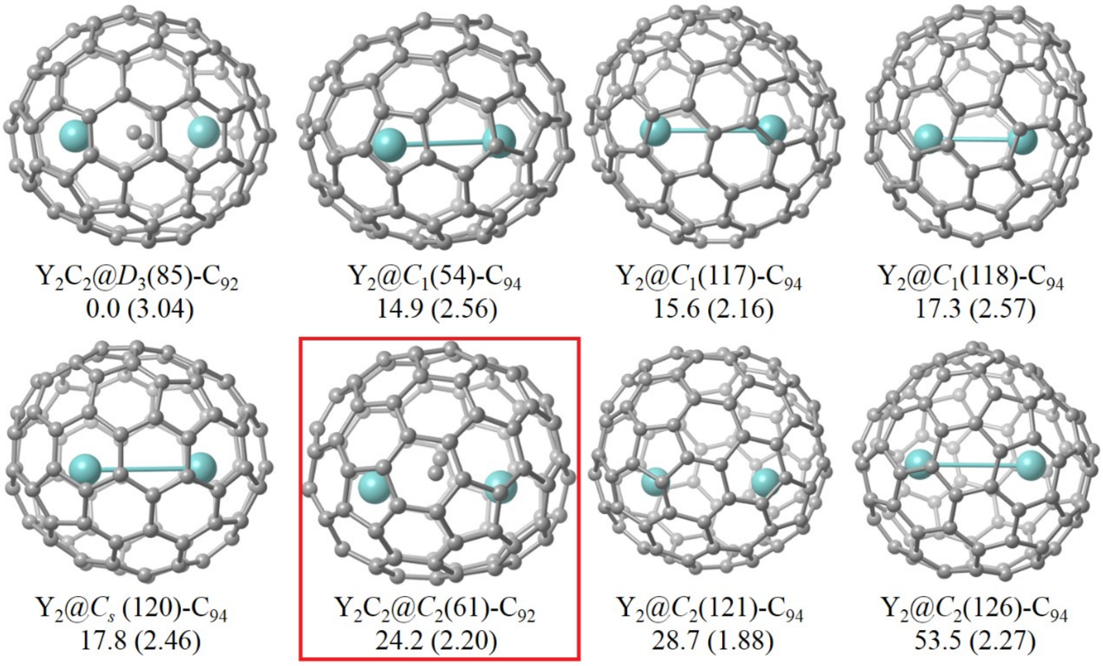

Figure S16. Optimized structures of low-energy Y_2C_{94} isomers with relative energies (kcal/mol) and HOMO-LUMO gap energies (eV, in parenthesis). The isomer marked with a red box is experimentally obtained.

Table S6. Interatomic distances ($R_{\text{Y-Y}}$, Å), Wiberg bond orders (WBOs), electron occupancies (Occ., *e*), natural population analysis charges and natural electron configuration populations of the two Y atoms of other Y_2@C_{2n} isomers.

Species	$R_{\text{Y-Y}}$	**WBO**	**Occ.**	**Atom**[a]	**Charge**	**Population**	**Hybrid composition**
Y_2@C_s(32)-C_{88}	4.18	1.05	1.98	Y1	1.17	$5s^{0.65}4d^{0.44}5p^{0.53}6s^{0.01}6p^{0.01}6d^{0.11}$	s(58%)p(31%)d(11%)
				Y2	1.10	$5s^{0.53}4d^{0.55}5p^{0.60}6s^{0.01}6p^{0.01}6d^{0.18}$	s(47%)p(35%)d(18%)
Y_2@C_1(26)-C_{88}	4.04	1.06	1.98	Y1	1.12	$5s^{0.52}4d^{0.56}5p^{0.60}6s^{0.01}6p^{0.01}6d^{0.16}$	s(46%)p(35%)d(19%)
				Y2	1.16	$5s^{0.61}4d^{0.48}5p^{0.55}6s^{0.01}6p^{0.01}6d^{0.03}$	s(54%)p(32%)d(14%)
Y_2@C_1(30)-C_{88}	4.16	1.05	1.97	Y1	1.12	$5s^{0.59}4d^{0.51}5p^{0.57}6s^{0.01}6p^{0.01}6d^{0.16}$	s(52%)p(33%)d(15%)
				Y2	1.12	$5s^{0.55}4d^{0.52}5p^{0.59}6s^{0.01}6p^{0.01}6d^{0.17}$	s(50%)p(35%)d(15%)
Y_2@C_s(31)-C_{88}	4.86	0.26		Y1	1.55	$5s^{0.19}4d^{0.58}5p^{0.42}6s^{0.02}6d^{0.23}$	
				Y2	1.42	$5s^{0.20}4d^{0.63}5p^{0.36}6s^{0.02}6p^{0.12}6d^{0.20}$	
Y_2@C_1(80982)-C_{88}	4.87	0.25		Y1	1.43	$5s^{0.20}4d^{0.61}5p^{0.36}6s^{0.01}6p^{0.11}6d^{0.28}$	
				Y2	1.56	$5s^{0.20}4d^{0.56}5p^{0.42}6s^{0.02}6d^{0.23}$	
Y_2@C_2(28)-C_{88}	4.30	1.04	1.98	Y1	1.14	$5s^{0.60}4d^{0.49}5p^{0.55}6s^{0.01}6p^{0.01}6d^{0.17}$	s(54%)p(32%)d(14%)
				Y2	1.14	$5s^{0.60}4d^{0.49}5p^{0.55}6s^{0.01}6p^{0.01}6d^{0.17}$	s(54%)p(32%)d(14%)
Y_2@D_2(35)-C_{88}	4.77	0.14		Y1	1.67	$5s^{0.11}4d^{0.63}5p^{0.24}6s^{0.02}6p^{0.10}6d^{0.18}$	
				Y2	1.67	$5s^{0.11}4d^{0.63}5p^{0.24}6s^{0.02}6p^{0.10}6d^{0.18}$	
Y_2@C_2(43)-C_{90}	3.90	1.07	1.97	Y1	1.14	$5s^{0.54}4d^{0.55}5p^{0.58}6s^{0.01}6p^{0.01}6d^{0.16}$	s(48%)p(34%)d(18%)
				Y2	1.14	$5s^{0.54}4d^{0.55}5p^{0.58}6s^{0.01}6p^{0.01}6d^{0.16}$	s(48%)p(34%)d(18%)
Y_2@C_1(21)-C_{90}	3.90	1.03	1.93	Y1	1.18	$5s^{0.52}4d^{0.54}5p^{0.56}6s^{0.01}6p^{0.01}6d^{0.16}$	s(48%)p(34%)d(18%)
				Y2	1.13	$5s^{0.53}4d^{0.54}5p^{0.60}6s^{0.01}6p^{0.01}6d^{0.16}$	s(47%)p(36%)d(17%)
Y_2@C_2(44)-C_{90}	3.79	1.08	1.97	Y1	1.17	$5s^{0.55}4d^{0.54}5p^{0.56}6s^{0.01}6p^{0.01}6d^{0.16}$	s(49%)p(33%)d(18%)
				Y2	1.17	$5s^{0.55}4d^{0.54}5p^{0.56}6s^{0.01}6p^{0.01}6d^{0.16}$	s(49%)p(33%)d(18%)
Y_2@C_2(41)-C_{90}	4.32	1.04	1.98	Y1	1.14	$5s^{0.69}4d^{0.44}5p^{0.54}6s^{0.01}6p^{0.01}6d^{0.06}$	s(59%)p(29%)d(12%)
				Y2	1.18	$5s^{0.51}4d^{0.53}5p^{0.56}6s^{0.01}6p^{0.01}6d^{0.16}$	s(48%)p(35%)d(17%)
Y_2@C_2(42)-C_{90}	4.37	1.02	1.96	Y1	1.20	$5s^{0.45}4d^{0.56}5p^{0.56}6s^{0.01}6p^{0.01}6d^{0.17}$	s(44%)p(36%)d(20%)
				Y2	1.14	$5s^{0.77}4d^{0.41}5p^{0.49}6s^{0.01}6p^{0.01}6d^{0.01}$	s(66%)p(25%)d(9%)
Y_2@D_3(85)-C_{92}	4.54	1.02	1.98	Y1	1.17	$5s^{0.63}4d^{0.44}5p^{0.53}6s^{0.01}6p^{0.01}6d^{0.13}$	s(58%)p(31%)d(11%)

				Y2	1.16	$5s^{0.65}4d^{0.44}5p^{0.52}6s^{0.01}6p^{0.01}6d^{0.08}$	s(59%)p(31%)d(10%)
$Y_2@C_2(64)$-C_{92}	4.39	1.03	1.98	Y1	1.14	$5s^{0.61}4d^{0.48}5p^{0.55}6s^{0.01}6p^{0.01}6d^{0.16}$	s(55%)p(32%)d(13%)
				Y2	1.14	$5s^{0.61}4d^{0.48}5p^{0.55}6s^{0.01}6p^{0.01}6d^{0.16}$	s(55%)p(32%)d(13%)
$Y_2@C_1(66)$-C_{92}	3.76	1.09	1.98	Y1	1.16	$5s^{0.58}4d^{0.51}5p^{0.57}6s^{0.01}6p^{0.01}6d^{0.16}$	s(51%)p(33%)d(16%)
				Y2	1.12	$5s^{0.52}4d^{0.58}5p^{0.61}6s^{0.01}6p^{0.01}6d^{0.15}$	s(45%)p(35%)d(20%)
$Y_2@T(86)$-C_{92}	4.26	1.04	1.98	Y1	1.16	$5s^{0.60}4d^{0.47}5p^{0.57}6s^{0.01}6p^{0.01}6d^{0.08}$	s(54%)p(33%)d(13%)
				Y2	1.16	$5s^{0.60}4d^{0.47}5p^{0.57}6s^{0.01}6p^{0.01}6d^{0.11}$	s(54%)p(33%)d(13%)
$Y_2@C_2(65)$-C_{92}	4.95	0.16		Y1	1.62	$5s^{0.13}4d^{0.62}5p^{0.37}6s^{0.02}6p^{0.01}6d^{0.23}$	
				Y2	1.62	$5s^{0.13}4d^{0.62}5p^{0.37}6s^{0.02}6p^{0.01}6d^{0.23}$	
$Y_2@C_s(16)$-C_{92}	3.34	1.17	1.98	Y1	1.18	$5s^{0.01}4d^{0.29}5p^{0.59}6s^{0.53}6p^{0.01}6d^{0.36}$	s(46%)p(36%)d(18%)
				Y2	1.18	$5s^{0.01}4d^{0.29}5p^{0.59}6s^{0.53}6p^{0.01}6d^{0.36}$	s(46%)p(36%)d(18%)
$Y_2@C_1(54)$-C_{94}	3.96	1.05	1.96	Y1	1.14	$5s^{0.56}4d^{0.55}5p^{0.56}6s^{0.01}6p^{0.01}6d^{0.11}$	s(49%)p(32%)d(19%)
				Y2	1.18	$5s^{0.56}4d^{0.50}5p^{0.55}6s^{0.01}6p^{0.01}6d^{0.16}$	s(52%)p(32%)d(16%)
$Y_2@C_1(117)$-C_{94}	4.47	1.02	1.97	Y1	1.15	$5s^{0.63}4d^{0.47}5p^{0.54}6s^{0.01}6p^{0.01}6d^{0.12}$	s(57%)p(31%)d(12%)
				Y2	1.15	$5s^{0.63}4d^{0.47}5p^{0.54}6s^{0.01}6p^{0.01}6d^{0.12}$	s(57%)p(31%)d(12%)
$Y_2@C_1(118)$-C_{94}	3.84	1.09	1.98	Y1	1.15	$5s^{0.53}4d^{0.55}5p^{0.58}6s^{0.01}6p^{0.01}6d^{0.15}$	s(47%)p(35%)d(18%)
				Y2	1.19	$5s^{0.60}4d^{0.49}5p^{0.55}6s^{0.01}6p^{0.01}6d^{0.14}$	s(53%)p(32%)d(15%)
$Y_2@C_s(120)$-C_{94}	4.37	1.01	1.95	Y1	1.15	$5s^{0.73}4d^{0.44}5p^{0.49}6s^{0.01}6p^{0.01}6d^{0.01}$	s(64%)p(26%)d(10%)
				Y2	1.21	$5s^{0.51}4d^{0.51}5p^{0.55}6s^{0.01}6p^{0.01}6d^{0.17}$	s(50%)p(34%)d(15%)
$Y_2@C_2(121)$-C_{94}	4.63	0.40		Y1	1.44	$5s^{0.23}4d^{0.63}5p^{0.47}6s^{0.02}6p^{0.01}6d^{0.17}$	
				Y2	1.44	$5s^{0.23}4d^{0.63}5p^{0.47}6s^{0.02}6p^{0.01}6d^{0.17}$	
$Y_2@C_2(126)$-C_{94}	4.44	1.03	1.98	Y1	1.17	$5s^{0.63}4d^{0.46}5p^{0.54}6s^{0.01}6p^{0.01}6d^{0.11}$	s(57%)p(32%)d(11%)
				Y2	1.17	$5s^{0.63}4d^{0.46}5p^{0.54}6s^{0.01}6p^{0.01}6d^{0.11}$	s(57%)p(32%)d(11%)

---

[a] The Y atoms are numbered from left to right in Figures S13-S16.

References

S1 Q. Q. Tang, L. Abella, Y. J. Hao, X. H. Li, Y. B. Wan, A. Rodríguez-Fortea, J. M. Poblet, L. Feng and N. Chen, *Inorg. Chem.*, 2015, **54**, 9845-9852.

S2 C. H. Chen, L. Abella, M. R. Cerón, M. A. Guerrero-Ayala, A. Rodríguez-Fortea, M. M. Olmstead, X. B. Powers, A. L. Balch, J. M. Poblet and L. Echegoyen, *J. Am. Chem. Soc.*, 2016,

138, 13030-13037.

S3 D. Lei, C. Zhao and L. H. Gan, *Acta Chim. Sinica,* 2014, **72**, 1105-1109.

S4 Y. X. Gu, Q. Z. Li, D. H. Li, R. S. Zhao and X. Zhao, *Chem. Phys. Lett.,* 2018, **698**, 77-84.

S5 R. Zhao, K. Yuan, S. D. Zhao, X. Zhao and M. Ehara, *Inorg. Chem.*, 2017, **56**, 11883-11890.

S6 A. A. Popov and L. Dunsch, *J. Am. Chen. Soc.*, 2007, **129**, 11835-11849.